

Numerical simulations of the radiative transfer in a 2D axisymmetric turbulent non-premixed methane–air flame using up-to-date WSGG and gray-gas models

Felipe Roman Centeno¹ · Cristiano Vitorino da Silva² · Rogério Brittes¹ · Francis H. R. França¹

Received: 1 April 2015 / Accepted: 1 September 2015 / Published online: 14 September 2015
© The Brazilian Society of Mechanical Sciences and Engineering 2015

Abstract This paper presents a study of the effect of thermal radiation in the simulation of a turbulent, non-premixed methane–air flame. In such a problem, modeling of radiative properties of the gaseous mixture is a fundamental aspect to be evaluated. In this work, such properties were modeled using three different models [a constant-ratio (CR-) and a non-constant-ratio (NCR-) weighted-sum-of-gray-gases (WSGG); and a gray-gas (GG) model], both based on newly obtained correlations from HITEMP 2010 database. The chemical reaction rates were considered as the minimum values between Arrhenius and Eddy Break-Up rates. A two-step global reaction mechanism was used, while the turbulence modeling was considered via standard k – ϵ model. The source terms of the energy equation consisted of the heat generated in the chemical reaction rates as well as in the radiation exchanges. The discrete ordinates method (DOM) was employed to solve the radiative transfer equation (RTE), including the TRI. Comparisons of simulations with/without radiation demonstrated that the temperature, the radiative heat source, and the wall heat flux were importantly affected by thermal radiation, while the influence on species concentrations proved to be less important. The numerical results considering radiation in the analysis were closer to the experimental data from literature when compared to the case neglecting it;

the computation of radiation with both the CR-WSGG and NCR-WSGG models provided better results than GG model, when compared with experimental data. For the combustion chamber and turbulence and combustion models employed in the present work, it was shown that the CR-WSGG is the recommended model, due to the acceptable agreement with experimental data and relatively low computational requirements in comparison to the NCR-WSGG model. The results show the importance of thermal radiation for an accurate prediction of the thermal behavior of a combustion chamber.

Keywords Radiation heat transfer · WSGG model · GG model · Combustion

1 Introduction

Combustion problems involve a number of coupled phenomena, such as fluid mechanics, heat transfer, and chemical kinetics of gaseous species and soot, in which thermal radiation can be the dominant heat transfer mode. Heat transfer directly affects the temperature field and, therefore, the chemical kinetics. Therefore, an accurate description of radiative heat transfer is of great importance for simulations of combustion systems. On the other hand, modeling thermal radiation exchanges in combustion gases (such as water vapor and carbon dioxide) is a difficult task due to the highly complex dependence of the absorption coefficient with the wavenumber, which is typically characterized by hundreds of thousands or millions of spectral lines. Thus, the integration of the radiative transfer equation (RTE) over the spectrum would be very expensive or even impossible without the use of spectral models. As a first simplification, the RTE is frequently solved with the gray-gas (GG)

Technical Editor: Luis Fernando Figueira da Silva.

✉ Francis H. R. França
frfranca@mecanica.ufrgs.br

¹ Department of Mechanical Engineering, Federal University of Rio Grande do Sul, Porto Alegre, RS, Brazil

² Universidade Regional Integrada do Alto Uruguai e das Missões-URI, Erechim, RS, Brazil

model, where the dependence of the absorption coefficient over the wavenumber is simply neglected. To provide realistic results, more refined models are however needed. As one advance to the GG model, the weighted-sum-of-gray-gases (WSGG) [1] makes perhaps the best compromise between accuracy and computation demand, especially in global simulation of combustion processes in which the RTE is solved together with fluid flow, chemical kinetics and energy equation. In the WSGG model, the entire spectrum is represented by a few bands having uniform absorption coefficients, each band corresponding to a gray gas. The weighting coefficients account for the contribution of each gray gas, such as in [2, 3]. In a recent study, Demarco et al. [4] assessed several radiative models, such as the narrow band, wide band, GG and global models such as the WSGG and spectral-line-based WSGG (SLW). According to the authors, the WSGG is very efficient from a computational point of view, and can yield accurate predictions. Simplified radiative property models, such as the WSGG or GG models, are often used in computational fluid dynamics (CFD) to simulate combustion problems. The main reason is that implementing more sophisticated models may become excessively time consuming when fluid flow/combustion/radiative heat transfer are coupled. Examples of works applying those models can be found in Watanabe et al. [5], where it was presented a numerical simulation of turbulent spray combustion to predict the combustion behavior in a jet burner taking into account thermal radiation by means of the WSGG model; in Bidi et al. [6], where the RTE was solved using the WSGG model to compute non-gray radiation in combustion gases in a cylindrical chamber; in Bazdidi-Tehrani and Zeinivand [7], who investigated a two-phase reactive flow corresponding to a diesel oil–air flame to predict the turbulent flow behavior and the temperature distribution; and the investigation on the effect of turbulence and radiation models on combustion characteristics in propane–hydrogen diffusion flames reported in Yilmaz et al. [8]. Crnomarkovic et al. [9] compared the numerical results obtained when the GG and the WSGG models were applied to model the radiative properties of the gas phase inside a lignite fired furnace. In Yadav et al. [10], the combustion processes of turbulent non-premixed pilot stabilized flames were studied including radiative heat transfer by means of the WSGG model. In Silva et al. [11], the authors applied the GG model to study the combustion of coal in a commercial thermal power plant to simulate the operational conditions and identify the factors of inefficiency.

Several researchers have studied new WSGG correlations for application in combustion systems. Taking into account that a limitation of the WSGG is that its correlations coefficients are generally established for a particular ratio of partial pressures for CO_2 and H_2O mixtures,

Krishnamoorthy [12] obtained new WSGG parameters computed from total emissivity correlations encompassing the range of the $\text{H}_2\text{O}/\text{CO}_2$ ratios encountered within Sandia Flame D. With the same motivation, Johansson et al. [13] modified the WSGG to account for various ratios of H_2O and CO_2 concentrations, covering from oxyfuel combustion of coal to combustion of natural gas.

One important advance in the modeling of radiation in participating gas was the establishment in the past century of high-resolution spectral database that provides spectroscopic parameters to generate the transition lines, such as HITRAN, built at a reference temperature of 296 K for atmospheric applications, and HITEMP, which was established for high-temperature applications. Recently, HITEMP 2010 [14] was released as a major improvement of previous versions, expanding the number of transition lines for H_2O and CO_2 , and also allowing for application in temperatures up to 4000 K. In recent works, Kangwanpongpan et al. [15] considered the determination and evaluation of new correlations for the WSGG model, fitted from emittance charts calculated from the up-to-date HITEMP 2010 database, to predict the radiative transfer in gases under oxyfuel conditions, while Dorigon et al. [16] generated correlations for typical ratios of partial pressures of the products of combustion of methane and fuel oil. Cassol et al. [17] developed new coefficients for the WSGG based on HITEMP 2010 but with a methodology that provides separate coefficients for H_2O and CO_2 , together with a methodology that allows the mixture of any concentration of those chemical species. Cassol et al. [18] fitted temperature-dependent coefficients for a GG model also based on HITEMP 2010 data.

This study presents a numerical RANS (Reynolds Average Navier–Stokes) simulation of turbulent non-premixed methane–air flame in a cylindrical combustion chamber taking into account radiation effect of non-gray gases by means of different WSGG [16, 17] and GG [18] correlations both generated from HITEMP 2010 database [14] and including TRI [19], with the objective of evaluating the influence of the different radiation models on the overall thermal behavior of the combustion chamber. For evaluation of the proposed solution, the case described in [20] was studied, since detailed spatial measurements are available for the main gas species concentrations and for the temperature field. Previous works demonstrated: (1) the importance of using updated WSGG coefficients for constant ratios of partial pressures of H_2O and CO_2 in relation to old coefficients [21]; and (2) the importance of computing TRI effects [22]. The present study investigates the effect of using different WSGG models: CR-WSGG, which considers a constant ratio between the H_2O and CO_2 partial pressures, and the NCR-WSGG, which considers a non-constant ratio. The analysis also presents the use of an updated

gray-gas model, which is still often used in combustion simulations. In all cases, TRI effects are considered. It is expected that the results presented in this paper will provide a guide for the choice of the radiative gas model in the simulation of combustion processes.

2 Problem statement

The physical system consists of the natural gas combustion chamber described in [20], which presents several challenges for radiation modeling in the sense that the flame is turbulent, and with highly non-isothermal, non-homogeneous medium. Several experimental data for temperature and species concentrations profiles along axial and radial coordinates were presented in [20], in addition to the results provided in the investigations of [23–25], making it a good test case for the methodology that is presented in the current study.

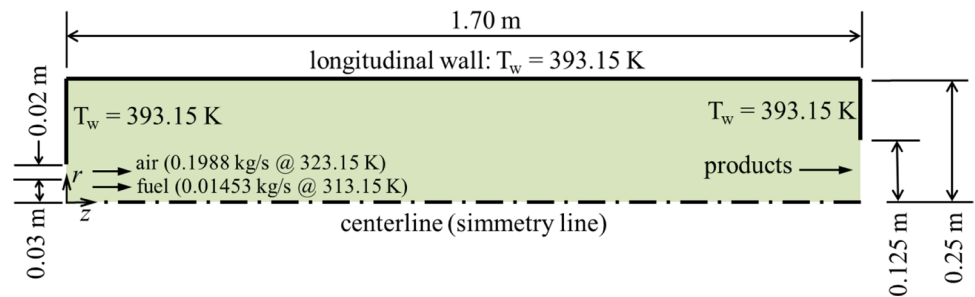
Keeping the same conditions as described in [20], the cylindrical chamber has length and diameter of 1.7 m and 0.5 m, respectively, as shown in Fig. 1. Natural gas is injected into the chamber by a duct aligned with the chamber centerline, leading to a non-swirling flame. In all cases, a fuel excess of 5 % (equivalence ratio of 1.05) was prescribed. For a fuel mass flow rate of 0.01453 kg/s at a temperature of 313.15 K, this requires an air mass flow rate of 0.1988 kg/s, at a temperature of 323.15 K. The fuel enters the chamber through a cylindrical duct having 0.06 m diameter, while air enters the chamber through a centered annular duct having a spacing of 0.02 m. For such mass flow rates, the fuel and air velocities are 7.23 and 36.29 m/s, respectively. The Reynolds number at the entrance (weighted for the air–fuel streams) is 1.8×10^4 . The inlet air is composed of oxygen (23 % in mass fraction), nitrogen (76 %) and water vapor (1 %), while the fuel is composed of 90 % of methane and 10 % of nitrogen. The operational pressure of the chamber is 101,325 Pa (1 atm). The burner power is about 600 kW. Buoyancy effects are neglected due to the high velocities that are provided by the burner. Figure 1 also depicts the symmetry

in the centerline and prescribed temperature on the walls (393.15 K). In addition, impermeability and no-slip conditions were assumed on the walls. In the symmetry line, it was assumed that both radial velocity and velocity gradient were null. The same procedure was adopted for the turbulent kinetic energy and its dissipation rate, enthalpy, and species concentrations in the symmetry line. In the outlet, null diffusive fluxes were assumed for all variables, the axial velocity component was corrected by a factor to satisfy mass conservation, and the radial velocity was imposed to be null. Both chamber walls, inlet and the outlet ducts were modeled as black surfaces. The temperature at the outlet duct was equal to the outlet flow bulk temperature. In the inlet, the velocity and concentration profiles were assumed uniform in the axial direction, while the turbulent kinetic energy was computed as $k = 1.5(u_{in}i)^2$, where i is the turbulence intensity (6 and 10 % for the air and for the fuel streams) and u_{in} is the inlet axial mean velocity, and for the turbulent kinetic energy dissipation rate, the relation $\varepsilon = \left(C_{\mu}^{3/4} k^{3/2} \right) / l$ was employed, where l is the turbulence characteristic length scale (0.04 and 0.03 m for the air and the fuel streams). For both energy and momentum conservation equations, standard wall functions were applied for the combustor walls treatment [26].

3 Mathematical formulation

The proposed work is stated as: considering a steady turbulent non-premixed methane–air flame in a cylindrical chamber, compute the temperature, species concentrations and velocity fields, and verify the influence of radiation on the process. To do that, it is taking into account a WSGG model with correlations obtained for a fixed ratio between the concentrations of the participating species [16], a WSGG model with correlations that allow variations in the concentration ratios [17], and a sophisticated gray-gas model which allows temperature dependence for the absorption coefficient [18], both based on HITEMP 2010 data [14].

Fig. 1 Combustion chamber geometry



3.1 Governing equations

Conservation equations for mass, momentum in the axial and radial directions, k - ε turbulence model, energy, and chemical species mass fractions (CH_4 , O_2 , CO_2 , CO , H_2O) for steady low-Mach flow in 2D axisymmetric coordinates are solved. Detailed information about governing equations can be found in [22].

3.2 Combustion kinetics

As a basic assumption, it is considered that the combustion process occurs at finite rates with methane oxidation taking two global steps: $2\text{CH}_4 + 3(\text{O}_2 + 3.76\text{N}_2) \rightarrow 2\text{CO} + 4\text{H}_2\text{O} + 11.28\text{N}_2$ and $2\text{CO} + (\text{O}_2 + 3.76\text{N}_2) \rightarrow 2\text{CO}_2 + 3.76\text{N}_2$.

The rate of formation or consumption, $R_{\alpha,c}$, of each α -th species in each c -th reaction (there are two reactions, so $c = 2$) is obtained by the Arrhenius–Magnussen’s model [27–29], in which the rate of formation or consumption of the chemical species is taken as the smallest one between the values obtained from Arrhenius kinetics (finite rate chemistry—FRC) or from Magnussen’s equations (Eddy Break-Up—EBU) [30]. In Magnussen’s model, the chemical reaction rate is governed by the large-eddy mixing time scale, k/ε , while combustion proceeds whenever turbulence is present ($k/\varepsilon > 0$). In the model, the Arrhenius rate acts as a kinetic “switch”; once the flame is ignited, the Magnussen’s rate is generally smaller than the Arrhenius rate, so reactions are mixing-limited [29]. The investigation in Silva et al. [23], which considered the same combustion chamber, provided the relative importance of the combustion kinetics by computing the Damköhler number, and found that the combustion process is governed by Arrhenius rates in the flame core and by Magnussen’s rates in all the other regions. This formulation was also successfully employed in [21–23, 25]. Also, the chemistry described above does not involve soot formation/oxidation, considering that the methane flame is low sooting. However, it should be recognized that even small quantities of soot can affect the radiation heat transfer, so the inclusion of soot into the analysis is one possible advance for future researches.

3.3 Radiation modeling

The radiative transfer equation (RTE) for non-scattering media, in cylindrical coordinates, with the discrete ordinates method (DOM), is given by:

$$\frac{\partial I_\eta}{\partial s} = \mu \frac{\partial I_\eta}{\partial r} + \xi \frac{\partial I_\eta}{\partial z} - \frac{\zeta}{r} \frac{\partial I_\eta}{\partial \phi} = -\kappa_\eta I_\eta + \kappa_\eta I_{\eta b} \quad (1)$$

Subjected to boundary conditions for diffusively emitting and reflecting opaque surface:

$$I_{\eta w} = \varepsilon_{\eta w} I_{\eta b}(T_w) + \frac{(1 - \varepsilon_{\eta w})}{\pi} \int_{\hat{n} \cdot \hat{s}} I_\eta |\hat{n} \cdot \hat{s}| d\Omega \quad (2)$$

where μ , ζ , and ξ are the directions, η is the wavenumber, I_η is the spectral intensity, $I_{\eta b}$ is the blackbody spectral intensity, $\varepsilon_{\eta w}$ is the wall emissivity, \hat{n} and \hat{s} are the vector normal to the surface element and the vector in the direction of the radiation intensity, respectively, Ω is the solid angle, T_w is the wall temperature, and κ_η is the spectral absorption coefficient. In the right side of Eq. (1), the first and the second terms represent, respectively, attenuation due to absorption and augmentation due to emission. Once the RTE is solved, the radiative heat source, presented in the energy equation as S_{rad} , is calculated as:

$$S_{\text{rad}} = -\nabla \cdot \vec{q}_r = \int_{\Omega} \int_{\eta} (\kappa_\eta I_\eta - \kappa_\eta I_{\eta b}) d\eta d\Omega \quad (3)$$

where \vec{q}_r is the radiative heat flux. The spectral absorption coefficient (κ_η) is strongly dependent on the wavenumber, which for participating gases can involve several thousands or millions of spectral lines. Therefore, solving Eq. (1) for all spectral lines is in general excessively time consuming for coupled solutions of the conservation equations. As such, gas models have been developed to solve the RTE quickly. A brief description of each gas model selected for the present analysis, the WSGG and the gray-gas models is presented in Sects. 3.4–3.6.

3.4 The constant-ratio weighted-sum-of-gray-gases (CR-WSGG) model

The original formulation of the WSGG model [1] consists of expressing the total gas emittance by weighted-sum-of-gray-gas emittances. The emission weighted factors, $a_j(T)$, and the absorption coefficients, κ_j , for the j^{th} gray gas are in general determined from the best fit of the total emittance with the constraint that the a_j must sum to 1. From a more general point of view, the WSGG model can be applied as a non-gray-gas model [31], solving the RTE for the N_G (number of gray gases) plus one ($j = 0$, representing spectral windows where H_2O and CO_2 are transparent to radiation):

$$\frac{dI_j}{ds} = -\kappa_j I_j + \kappa_j a_j(T) I_b(T) \quad (4)$$

In which $I_b(T) = \sigma T^4 / \pi$ (σ is the Stefan–Boltzmann constant) and the emission weighted factor $a_j(T)$ is given by,

$$a_j(T) = \sum_{i=1}^5 b_{j,i} T^{i-1} \quad (5)$$

Table 1 Coefficients of the WSGG model [16], $p_{H_2O}/p_{CO_2} = 2$

j	$\kappa_{p,j}$ [m ⁻¹ atm ⁻¹]	$b_{j,1} \times 10^1$	$b_{j,2} \times 10^4$ [K ⁻¹]	$b_{j,3} \times 10^7$ [K ⁻²]	$b_{j,4} \times 10^{10}$ [K ⁻³]	$b_{j,5} \times 10^{14}$ [K ⁻⁴]
1	0.192	0.5617	7.8440	-8.5630	4.2460	-7.4400
2	1.719	1.4260	1.7950	-0.1077	-0.6972	1.7740
3	11.370	1.3620	2.5740	-3.7110	1.5750	-2.2670
4	111.016	1.2220	-0.2327	-0.7492	0.4275	-0.6608

with j varying from 0 to N_G , and $I = \sum_{j=0}^{N_G} J_j$. The functional dependence of the weighted factors with temperature is generally fitted by polynomials, Eq. (5), where the polynomial coefficients ($b_{j,i}$) as well as the absorption coefficients for each gray gas can be tabulated. For H₂O/CO₂ mixtures, these coefficients are generally established for particular ratios of the partial pressure, p_{H_2O}/p_{CO_2} , which could limit the application of the method. In the present study, the weighted factors polynomial coefficients and absorption coefficients were taken from Dorigon et al. [16] for $p_{H_2O}/p_{CO_2} = 2$. Such WSGG correlations were fitted from HITEMP 2010 [14], which is the most recent molecular spectroscopic database for high temperatures. In the same study, Dorigon et al. [16] compared results obtained with the new coefficients against line-by-line (LBL) benchmark calculations for one-dimensional non-isothermal and non-homogeneous problems, finding maximum and average errors of about 5 and 2 % for radiative heat sources in different test cases. For convenience, Table 1 shows the pressure absorption coefficient $\kappa_{p,j}$ and coefficients $b_{j,i}$ obtained in [16]. The absorption coefficient of each gray gas in Eq. (4) can be computed from the pressure absorption coefficient by the following relation:

$$\kappa_j = (p_{H_2O} + p_{CO_2})\kappa_{p,j} \tag{6}$$

where p_{H_2O} and p_{CO_2} are the local partial pressures of H₂O and CO₂, respectively. This is one important aspect of the WSGG model, for it allows its ready application to non-homogeneous problems, in which the local partial pressure of the participating species varies from point to point in the computational domain. In this manner, besides the coefficients of the CR-WSGG being obtained for a constant ratio between partial pressures of H₂O and CO₂, it must be emphasized that this model is capable of taking into account inhomogeneity of H₂O and CO₂ concentrations inside the combustion chamber to compute the radiative transfer. Centeno et al. [21] tested the coefficients presented in Table 1 against old ones presented in [2] for an axisymmetric cylindrical combustion chamber, and found the new coefficients to make better agreement with experimental data. In this paper, the results from WSGG using the coefficients in Table 1 will be addressed as CR-WSGG (constant-ratio WSGG).

3.5 The non-constant-ratio weighted-sum-of-gray-gases (NCR-WSGG) model

Perhaps, the major limitation of the standard WSGG model is that the correlations are obtained for a fixed ratio between the partial pressures of the participating species, such as $p_{H_2O}/p_{CO_2} = 2$. There has been some recent works that propose an additional dimension to the correlations, in addition to the temperature dependence, to allow variations in the concentration ratios [13, 15, 32]. A different approach was proposed in [17], which obtained correlations separately for H₂O and CO₂, and then combined those correlations to solve mixtures with arbitrary ratios in the concentration.

According to [17], the weighting factor a_j can be interpreted as the probability that the energy of the blackbody is emitted in the regions of the spectrum where the absorption coefficient is κ_j . Therefore, the probability that the gray-gas absorption coefficient of the mixture is the sum of a given combination of the gray-gas absorption coefficients of the components will be equal to the product of their respective probabilities. Therefore, for a mixture of H₂O and CO₂:

$$\kappa_j = \kappa_{H_2O,j_{H_2O}} + \kappa_{CO_2,j_{CO_2}} \tag{7a}$$

$$a_j = a_{H_2O,j_{H_2O}} \times a_{CO_2,j_{CO_2}} \tag{7b}$$

where j_{H_2O} and j_{CO_2} represent one of the gray gases, respectively, for H₂O and CO₂. The absorption coefficients are computed as $\kappa_{H_2O,j} = p_{H_2O}\kappa_{p,H_2O,j}$ and $\kappa_{CO_2,j} = p_{CO_2}\kappa_{p,CO_2,j}$, where $\kappa_{p,H_2O,j}$ and $\kappa_{p,CO_2,j}$ are the pressure absorption coefficients for H₂O and CO₂. The gray-gas weighting coefficients $a_{H_2O,j_{H_2O}}$ and $a_{CO_2,j_{CO_2}}$ are computed according to Eq. (5), only replacing the coefficients $b_{j,i}$ by $b_{H_2O,j,i}$ and $b_{CO_2,j,i}$, respectively. The coefficients $\kappa_{p,H_2O,j}$, $\kappa_{p,CO_2,j}$, $b_{H_2O,j,i}$ and $b_{CO_2,j,i}$ obtained in [17] are presented in Tables 2 and 3. The correlations consider four gray gases for H₂O and CO₂, $J_{H_2O} = J_{CO_2} = 4$. In this paper, the results from WSGG using the coefficients in Tables 2 and 3 will be addressed as NCR-WSGG (non-constant-ratio WSGG). In Eqs. (7a) and (7b), the transparent windows of H₂O and CO₂ ($\kappa_{p,H_2O,0} = 0$ and $\kappa_{p,CO_2,0} = 0$) need to be considered, so $0 \leq j_{H_2O} \leq J_{H_2O}$, $0 \leq j_{CO_2} \leq J_{CO_2}$. For the mixture, the number of gray gases will be therefore

Table 2 Coefficients of the WSGG model for H₂O with four gray gases [17]

<i>j</i>	$\kappa_{p,H_2O,j} \text{ (atm}\cdot\text{m)}^{-1}$	$b_{H_2O,j,1} \times 10^1$	$b_{H_2O,j,2} \times 10^5 \text{ (K}^{-1}\text{)}$	$b_{H_2O,j,3} \times 10^8 \text{ (K}^{-2}\text{)}$	$b_{H_2O,j,4} \times 10^{11} \text{ (K}^{-3}\text{)}$	$b_{H_2O,j,5} \times 10^{15} \text{ (K}^{-4}\text{)}$
1	0.171	0.6617	55.48	−48.41	22.27	−40.17
2	1.551	1.1045	0.576	24.00	−17.01	30.96
3	5.562	−0.4915	70.63	−70.12	26.07	−34.94
4	49.159	2.3675	−18.91	−0.907	4.082	−8.778

Table 3 Coefficients of the WSGG model for CO₂ with four gray gases [17]

<i>j</i>	$\kappa_{p,CO_2,j} \text{ (atm}\cdot\text{m)}^{-1}$	$b_{CO_2,j,1} \times 10^1$	$b_{CO_2,j,2} \times 10^5 \text{ (K}^{-1}\text{)}$	$b_{CO_2,j,3} \times 10^8 \text{ (K}^{-2}\text{)}$	$b_{CO_2,j,4} \times 10^{11} \text{ (K}^{-3}\text{)}$	$b_{CO_2,j,5} \times 10^{15} \text{ (K}^{-4}\text{)}$
1	0.138	0.9990	64.41	−86.94	41.27	−67.74
2	1.895	0.0942	10.36	−2.277	−2.134	6.497
3	13.301	1.4511	−30.73	37.65	−18.41	30.16
4	340.811	−0.2915	25.23	−26.10	9.965	−13.26

Table 4 Absorption coefficients for the gray-gas model [18]

	<i>i</i> = CO ₂	<i>i</i> = H ₂ O
$c_0 \text{ (cm}^{-1}\text{atm}^{-1}\text{)}$	-6.4750×10^{-1}	7.5702×10^{-1}
$c_1 \text{ (cm}^{-1}\text{atm}^{-1}\text{K}^{-1}\text{)}$	4.2895×10^{-3}	-1.9716×10^{-3}
$c_2 \text{ (cm}^{-1}\text{atm}^{-1}\text{K}^{-2}\text{)}$	-6.6089×10^{-6}	2.1998×10^{-6}
$c_3 \text{ (cm}^{-1}\text{atm}^{-1}\text{K}^{-3}\text{)}$	4.4190×10^{-9}	-1.2492×10^{-9}
$c_4 \text{ (cm}^{-1}\text{atm}^{-1}\text{K}^{-4}\text{)}$	-1.3796×10^{-12}	3.5385×10^{-13}
$c_5 \text{ (cm}^{-1}\text{atm}^{-1}\text{K}^{-5}\text{)}$	1.6484×10^{-16}	-3.9663×10^{-17}

$J = (J_{H_2O} + 1) \times (J_{CO_2} + 1)$. Therefore, while the number of gray gases for the CR-WSGG model is $J = 4$, for the NCR-WSGG model the number of gray gases is increased to $J = 25$, increasing the computation time in about 6 times.

The application of the NCR-WSGG model to integrate the RTE in the spectrum is very similar to the CR-WSGG model. The only difference is that, prior to solving Eq. (4), the absorption coefficient and the weighting factor of each gray gas are obtained by means of Eqs. (7a) and (7b).

3.6 The gray-gas (GG) model

In the gray-gas model, the absorption coefficient is considered to be independent of the wavenumber and can be determined by an emission-based average along the spectrum. The gray-gas model is a quite simple implementation if compared with other spectral models due to the single constant absorption coefficient consideration. This approximation is unrealistic for gases, since they have a strong variation along the wavenumber, but it can still be found in modern studies on combustion [9, 11, 33] due to its simplicity.

To assist in the application of the gray-gas model, Cassol et al. [18] proposed new absorption coefficient correlations

for H₂O and CO₂, based on the up-to-date HITEMP 2010 database. The proposed temperature-dependent polynomial relation is presented in Eq. (8), while its coefficients are shown in Table 4. κ_i is the absorption coefficient for each species (H₂O or CO₂) and p_i is the partial pressure. The absorption coefficient of the mixture is obtained as $\kappa = \kappa_{H_2O} + \kappa_{CO_2}$. The RTE for the gray-gas model is similar to Eq. (4) but with $j = 1$.

$$\kappa_i = p_i \left(c_0 + c_1 T + c_2 T^2 + c_3 T^3 + c_4 T^4 + c_5 T^5 \right) \quad (8)$$

3.7 Turbulence–radiation interactions

The radiative transfer equation (RTE) is applicable to instant quantities that fluctuate in a turbulent flow, while the RANS turbulence model can only provide time-averaged (mean) quantities and, possibly, their mean square fluctuations. Considering the spectrally integrated form of the RTE, and time averaging, it results in:

$$\frac{d\bar{I}}{ds} = -\bar{\kappa} \bar{I} + \bar{\kappa} \bar{I}_b \quad (9)$$

The absorption coefficient–radiation intensity correlation, i.e., the first term in the right hand of Eq. (9) can be expressed as $\overline{\kappa I} = \bar{\kappa} \bar{I} + \overline{\kappa' I'}$. Several studies have neglected the second term on the right hand side of this expression ($\overline{\kappa' I'}$) based on arguments of Kabashnikov and Kmit [34], known as the optically thin fluctuation approximation (OTFA), which relies on the assumption that the absorption coefficient fluctuations are weakly correlated with the radiation intensity fluctuations, i.e., $\overline{\kappa' I'} \approx 0$, if the mean free path for radiation is much larger than turbulence integral length scale.

In the second term in the right hand of Eq. (9), which is proportional to $\overline{\kappa T^4}$, the instant values of κ and T correlate in a turbulent flow. In the present study, it is applied the

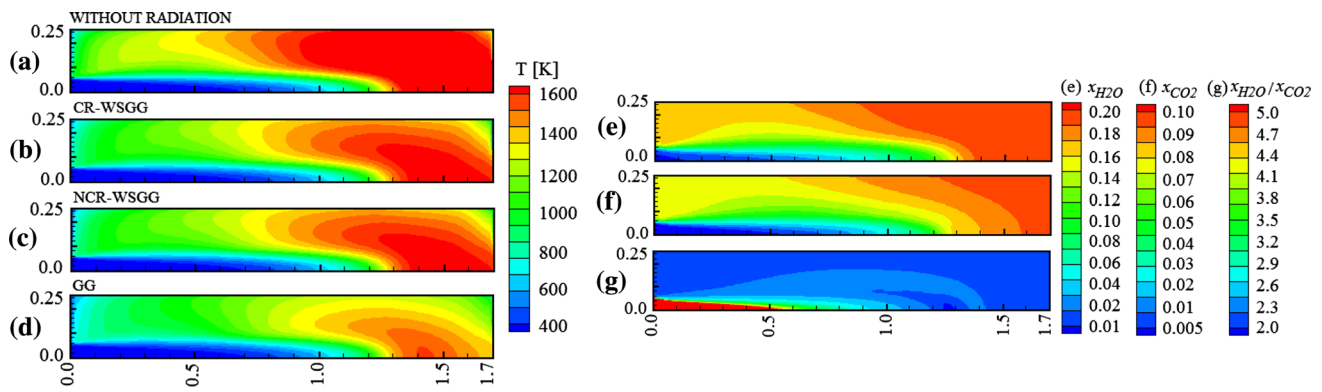


Fig. 2 Temperature fields: **a** radiation neglected; **b** radiation computed with the CR-WSGG model; **c** radiation computed with the NCR-WSGG model; **d** radiation computed with gray-gas (GG)

model. Chemical species mole fraction fields: **e** H₂O; **f** CO₂; **g** ratio between mole fractions of H₂O and CO₂

approximation proposed in Snegirev [19], in which both the absorption coefficient–temperature correlation and the temperature self-correlation are considered. These two TRI correlations were found to be the most important in reactive flows [35–37]. Decomposition of temperature and absorption coefficient into average and fluctuating components, $T = \bar{T} + T'$ and $\kappa = \bar{\kappa} + \kappa'$, followed by time averaging, and neglecting higher order terms, $\overline{\kappa T^4}$ can be written as [19]:

$$\overline{\kappa T^4} = \bar{\kappa} \cdot \bar{T}^4 \left(1 + C_{TRI} 6 \frac{\overline{T'^2}}{\bar{T}^2} + 4 \frac{\overline{T'^2}}{\bar{\kappa} \cdot \bar{T}} \frac{\partial \kappa}{\partial T} \bigg|_{\bar{T}} \right) \quad (10)$$

which allows the consideration of the absorption coefficient–temperature correlation and the temperature self-correlation. The value for C_{TRI} was initially suggested by [19] from data fitting for $\overline{T'^4}/\bar{T}^4$ and $\overline{T'^2}/\bar{T}^2$ as presented in Burns [38], followed by an adjustment leading to a value of 2.5 for C_{TRI} . To evaluate $\overline{T'^2}$, required for Eq. (10), an additional transport equation for temperature fluctuation variance is solved.

4 Results and discussions

The set of equations were solved using the finite volume method [26] by means of a Fortran code. The power law was applied as the diffusive–advective interpolation function on the faces of the control volumes. The pressure–velocity coupling was made by the SIMPLE method. The resulting system of algebraic equations was solved by the TDMA algorithm, with block correction in all equations except the equations for k and ϵ . A grid with 140 volumes in the axial direction and 48 volumes in the radial direction was used. The numerical accuracy was checked comparing predicted results calculated using this grid with results

obtained using coarser and thinner grids by means of a GCI (grid convergence analysis) study. As found, the 48×140 grid provided grid independent results, and required reasonable computational effort. The grid is uniformly spaced in both radial and axial directions. The radiative transfer calculations were performed using the same spatial grid, and S_6 quadrature. Convergence criteria were based on the imposition that the normalized residual mass in the simple method was 10^{-8} . For the other equations, the maximum relative variation between iterations was 10^{-6} .

To study the effect of the gas radiation heat transfer inside the combustion chamber, four different scenarios were considered. In the first scenario, radiation was completely ignored to analyze the importance of radiation in this particular flame simulation. In the second and third scenarios, radiation was considered with different WSGG models: CR-WSGG [16] and NCR-WSGG [17]. In the fourth scenario, radiation was computed with gray-gas model [18]. TRI was computed in both radiative scenarios using the approximation described above [19]. Comparisons were made to verify how the different radiative scenarios affect the temperature, H₂O and CO₂ mol fractions, and radiative heat source fields, as well as some of the thermal quantities, such as the radiant fraction and heat fluxes at chamber walls.

Figure 2a–d shows the results for temperature fields obtained for the four scenarios that were described above. Figure 2e–g shows the mole fraction distribution for the most important radiative chemical species, H₂O and CO₂, as well as the ratio between these two quantities. Figure 2e–g can be considered representative of any scenario, since H₂O and CO₂ mol fractions were not significantly affected by the different scenarios as will be discussed later.

As can be seen in Fig. 2a–d, consideration of the radiative transfer and different radiative properties models

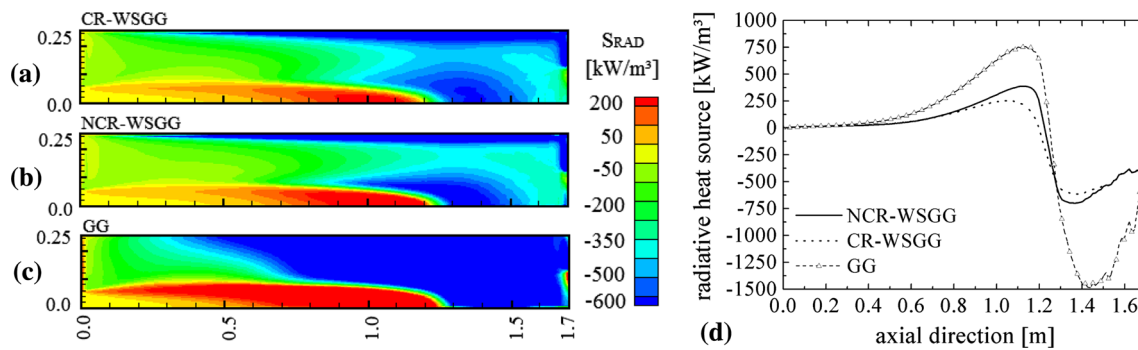


Fig. 3 Radiative heat source fields: **a** radiation computed with the CR-WSGG model; **b** radiation computed with the NCR-WSGG model; **c** radiation computed with the gray-gas (GG) model; **d** axial profiles of the radiative heat source along the chamber centerline

played an important role in the temperature field. Computed flame peak temperatures were 1809, 1679, 1678 and 1547 K for cases without radiation, and with radiation computed with CR-WSGG, NCR-WSGG and gray-gas, respectively. While these peaks were local, they can be taken as a measure to characterize the entire temperature field. The decrease in the peak temperature as a result of neglecting or considering radiative transfer (ΔT_{RAD}) is next analyzed. In the present study, the peak temperature dropped $\Delta T_{RAD} = 130, 131,$ and 262 K for radiation computed with CR-WSGG, NCR-WSGG and gray-gas, respectively. In similar investigation, Li and Modest [36] found a decrease of $\Delta T_{RAD} = 145$ K for a flame with an optical thickness of 0.474. The flame of the current study has an optical thickness of about 0.43, therefore with a slightly smaller influence of thermal radiation, so the differences between the studies are consistent when CR- and NCR-WSGGs were employed. Also, Poitou et al. [39] found drops of $\Delta T_{RAD} = 150$ K in the peak temperature for a propane–air turbulent diffusion flame. Peak temperature decreases are in agreement with literature data when CR-WSGG and NCR-WSGG were used, while gray-gas model provided overestimated peak temperature decreases.

Figure 2g shows the ratio x_{H_2O}/x_{CO_2} (which is equivalent to p_{H_2O}/p_{CO_2}) inside the chamber domain, where it is noted that almost the entire chamber has a ratio close to 2.0, which is an important aspect to model the radiative properties of the medium, especially when the CR-WSGG model is considered. Since this is an essentially emitting flame, the control volumes with temperature greater than approximately 1000 K are radiatively more important, since they are the emitting volumes, while the control volumes with temperature less than 1000 K are considered as the absorbing volumes. Great part of the control volumes with temperatures above 1000 K has the ratio x_{H_2O}/x_{CO_2} very close to 2.0, indicating that the use of WSGG correlations obtained for a fixed $x_{H_2O}/x_{CO_2} = 2$ ratio, as seen in Table 1, is in fact a reasonable choice.

Figure 3 shows the radiative heat source obtained for the second, third and fourth radiative scenarios, i.e., those scenarios in which thermal radiation was computed with CR-WSGG, NCR-WSGG and gray-gas model, respectively.

As with the temperature field, radiation fields also changed significantly as a result of the different radiative models (WSGG or gray-gas). The flame region with the highest temperatures emits more radiation than it absorbs, leading to negative heat sources, while the flame region with the smallest temperatures absorbs more radiation than it emits, leading to positive heat sources. As seen, the radiative heat source calculated with gray-gas model was in general higher than the one calculated with both WSGG models. The higher differences were located at a large region of the flame, with intermediate and high temperature levels and negative net radiative source (emitting region). Differences between the radiative heat sources computed with gray-gas (Fig. 3c) and WSGG models (Fig. 3a, b) reached 300 %, while the difference between CR-WSGG (Fig. 3a) and NCR-WSGG (Fig. 3b) is located in a very narrow region and reached a local maximum of 30 %. In addition, Fig. 3d shows S_{rad} profiles along axial direction at chamber centerline. From this figure, it is observed that the consideration of gray-gas model increased the absolute value of the radiative heat source, as also shown in Fig. 3a–c and as corroborated by the results that will be presented later in Tables 6 and 7. Besides, Centeno et al. [40] employed CR-WSGG and NCR-WSGG in a computation of the radiative heat source term using prescribed fields of temperature, H_2O and CO_2 , and found average and maximum errors of 1.6 and 8.5 % for the CR-WSGG and of 1.4 and 6.6 % for the NCR-WSGG, respectively, as compared to line-by-line calculations employing HITEMP 2010 database. From [40] results, it could be implied that errors related to gray-gas model, when comparing the radiative heat source term with line-by-line calculations, are much higher than those for CR- or NCR-WSGG models.

Fig. 4 Profiles of temperature at axial direction (*chamber centerline*) and at radial direction (at $z = 0.312$ m, $z = 0.912$ m, $z = 1.312$ m)

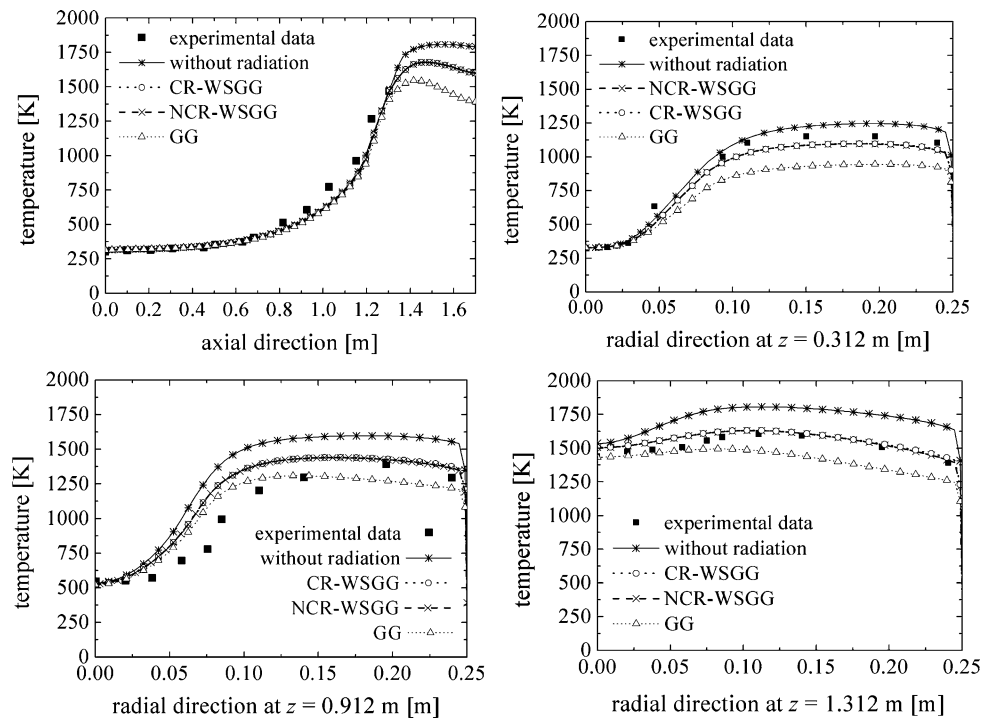
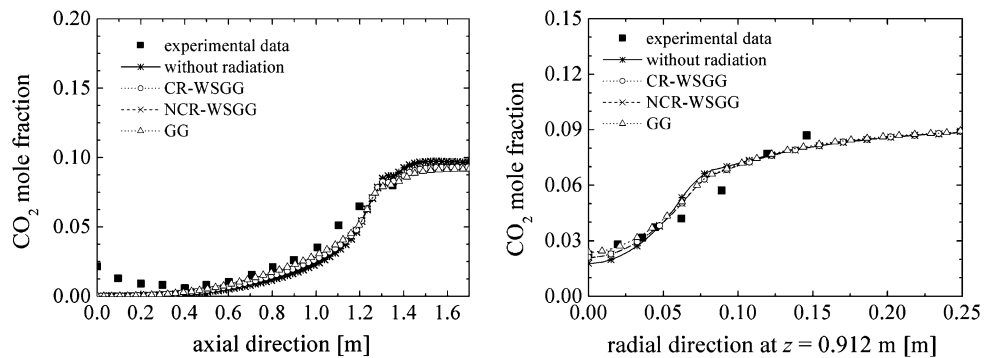


Fig. 5 Profiles of CO₂ mol fraction at axial direction (*chamber centerline*) and at radial direction (at $z = 0.912$ m)



Figures 4 and 5 show the temperature and CO₂ mol fraction profiles along the axial direction at the chamber centerline, and along the radial direction at axial positions of $z = 0.312$ m, $z = 0.912$ m, and $z = 1.312$ m from the chamber entrance, considering the scenarios described above together with the experimental data of Garréton and Simonin [20] (experimental data error bars are not available in [20]). One observes that the temperature values and temperature gradients decreased when radiation was considered since the heat transfer was improved. The same behavior is observed comparing results obtained with WSGG models and gray-gas model, that is, since computation of radiation with gray-gas model led to higher radiative transfer in comparison to the computation with WSGG models, the temperature and gradients reduced when gray-gas model was considered. The same analysis could be implied from Fig. 2. Since the reaction rate coefficients depend on the temperature, radiation should affect the formation and

consumption of the species involved in the process. In spite of this, the mean variations of CO₂ mol fractions using the different radiative scenarios were less than 1.0 %, showing that the species mole fractions were considerably less affected by the radiative modeling than the temperature. This could be caused by the use of EBU-FRC combustion model employed in the present study, in which chemical reaction rate is primarily controlled by turbulent mixing and, therefore, is less sensitive to temperature. On the other hand, the heat transfer rate through the chamber longitudinal wall, the net radiative heat loss and the radiant fraction strongly depended on the radiation modeling, as revealed in Figs. 2 and 3, and Tables 6 and 7. Figures 4 and 5 also show that for the radiation scenarios considering CR-WSGG and NCR-WSGG models, the mean temperature and mean mole fraction of CO₂ followed the experimental data trend despite some minor deviations. Those differences had probably minor relation to the choice of the radiation modeling,

Table 5 Average relative deviation expressing the temperature and CO₂ mol fraction difference between experimental data and numerical results for both radiative scenarios

	Without radiation	CR-WSGG	NCR-WSGG	gray-gas
Temperature: axial profile (Fig. 4)	2.6	2.8	2.8	3.6
Temperature: radial profile at $z = 0.312$ m (Fig. 4)	6.3	4.1	4.2	11.3
Temperature: radial profile at $z = 0.912$ m (Fig. 4)	18.1	10.3	10.1	9.2
Temperature: radial profile at $z = 1.312$ m (Fig. 4)	11.8	2.8	2.6	5.0
CO ₂ : axial profile (Fig. 5)	12.3	10.3	10.3	9.7
CO ₂ : radial profile at $z = 0.912$ m (Fig. 5)	6.7	4.6	4.7	4.7

Table 6 Heat transfer rate on the combustion chamber longitudinal wall

	Convective heat transfer rate [kW]	Radiative heat transfer rate [kW]	Total rate (radiation + convection) [kW]
without radiation	89.5	0.0	89.5
CR-WSGG	62.9	94.1	157.0
NCR-WSGG	63.1	94.0	157.1
Gray-gas	58.2	164.9	223.1

Table 7 Predicted net radiative heat loss and fraction of radiative heat loss

	Net radiative heat loss [kW]	Radiant fraction [%]
CR-WSGG	119.0	19.8
NCR-WSGG	119.2	19.8
Gray-gas	213.5	35.4

arising from limitations of the other models (turbulence and combustion models).

Table 5 presents the average relative deviation computed as $\%Dev = \sum_{i=1}^n \frac{1}{n} [100(V_{exp,i} - V_{rad,i}) / V_{exp,max}]$ expressing the difference between experimental data (V_{exp}) and numerical results (V_{rad}) (V can assume values of temperature or CO₂ mol fraction in the previous expression, and n is the total number of experimental data in each case) for both scenarios without radiation and with radiation computed with CR-WSGG, NCR-WSGG and gray-gas models, for all the results of Figs. 4 and 5. These deviations indicate that the major effect of radiation is on the temperature field, especially in the radial direction profiles, with minor effect on CO₂ mol fractions, which corroborates the results shown in Figs. 4 and 5.

An additional view of the effect of thermal radiation is presented in Table 6, which shows the heat transfer rates through the chamber longitudinal wall. The inclusion of thermal radiation has a major effect in the radiation–convection combined heat transfer mode, leading to an increase in the total heat transfer from 89.5 kW (only convection, without radiation heat transfer) to a maximum

of 223.1 kW (sum of convection and radiation heat transfer for the scenario with radiation computed with gray-gas model). It is interesting to note that when thermal radiation was included, the convective heat transfer decreased in comparison to the scenario in which thermal radiation was neglected, since the temperature gradients in the chamber were reduced. The results also show that the radiation heat transfer was increased when the gray-gas model was considered, as compared to WSGG model results, as expected since the radiative heat source (Fig. 3) was higher in that case. The net effect of the different models was an increase in the flame radiative emission, as seen in Fig. 3, and since the participant gaseous medium has an optical thickness relatively thin, higher flame radiative emission led in turn to higher radiative heat fluxes through the chamber walls.

The net radiative heat loss and its normalized variable, the radiant fraction (f_{rad}), are important quantities to describe the overall radiation field of the flame. The net radiative heat loss corresponds to the integral of S_{rad} over the computational domain, while the radiant fraction is the ratio of this value to the heat released in the combustion. In all simulation scenarios, these quantities were calculated; the results are shown in Table 7. As seen, the radiation loss and the corresponding radiant fraction from the present flame achieved significant values. It is observed in Table 7 that the net radiative heat loss and the radiant fraction were approximately the same for CR-WSGG and NCR-WSGG models, while for the gray-gas model they increased about 80 % when compared to both WSGG models.

As a final comment, the overall energy balance on the combustion chamber, as well as the radiative energy balance, was strictly verified in all simulations. The differences

between the radiative heat transfer rates reported in Table 6 and the net radiative heat losses reported in Table 7 were because the results in Table 6 are related only to radiative heat transfer on the longitudinal wall of the chamber, not taking into account the annular walls located at the entrance and exit of the chamber, as well as the inlet and outlet boundaries of the chamber.

5 Conclusions

This study presented an analysis of the thermal radiation in a turbulent non-premixed methane–air flame in a cylindrical combustion chamber. The radiation field was computed with different absorption coefficient models both based on the up-to-date HITEMP 2010 and considering TRI effects. A two-step global reaction mechanism was used and turbulence modeling was considered via standard k - ϵ model. The RTE was solved employing the discrete ordinates method. This work showed the importance of accurate predictions of the radiative heat transfer for combustion problems by means of four scenarios: radiation neglected from calculations, and radiation computed with CR-WSGG, NCR-WSGG and gray-gas models. The comparison of the results obtained from the different scenarios showed that the temperature (especially at high temperature regions), the radiative heat source, the heat transfer through chamber wall and the radiant fraction were importantly affected by the different scenarios, while radiation had minor importance in the prediction of the chemical species concentrations for the adopted chemical reaction model. The numerical results considering radiation in the analysis were closer to the experimental data [20] when compared to the case neglecting it; the computation of radiation with any WSGG (CR- or NCR-) provided better results than gray-gas model, when comparing present results with quantitative experimental data and with qualitative literature results. Therefore, for the combustion chamber and turbulence and combustion models employed in the present work, it was shown that the standard CR-WSGG is the most recommended to be employed, taking into account both accuracy and computational requirements. Some possible future advances in the radiation analysis are including kinetics for soot formation, a needed step prior to modeling combined soot and gas radiation.

Acknowledgments RB thanks to CNPq for a doctorate scholarship grant 140968/2011-3. FHRF thanks to CNPq for research grants 309961/2013-0 and 476490/2013-8.

References

- Hottel HC, Sarofim AF (1967) Radiative Transfer. McGraw-Hill, New York
- Smith TF, Shen ZF, Friedman JN (1982) Evaluation of coefficients for the weighted sum of gray gases model. *J Heat Transfer* 104:602–608
- Smith TF, Al-Turki AM, Byun KH, Kim TK (1987) Radiative and conductive transfer for a gas/soot mixture between diffuse parallel plates. *J Thermophys Heat Transfer* 1:50–55
- Demarco R, Consalvi JL, Fuentes A, Melis S (2011) Assessment of radiative property models in non-gray sooting media. *Int J Therm Sci* 50:1672–1684
- Watanabe H, Suwa Y, Matsushita Y, Morozumi Y, Aoki H, Tanno S, Miura T (2007) Spray combustion simulation including soot and NO formation. *Energy Convers Manag* 48:2077–2089
- Bidi M, Hosseini R, Nobari MRH (2008) Numerical analysis of methane–air combustion considering radiation effect. *Energy Convers Manag* 49:3634–3647
- Bazdidi-Tehrani F, Zeinivand H (2010) Presumed PDF modeling of reactive two-phase flow in a three dimensional jet-stabilized model combustor. *Energy Convers Manag* 51:225–234
- Yilmaz I, Taştan M, İlbaş M, Tarhan C (2013) Effect of turbulence and radiation models on combustion characteristics in propane–hydrogen diffusion flames. *Energy Convers Manag* 72:179–186
- Crnomarkovic N, Sijercic M, Belosevic S, Tucakovic D, Zivanovic T (2013) Numerical investigation of processes in the lignite-fired furnace when simple gray gas and weighted sum of gray gases models are used. *Int J Heat Mass Transf* 56:197–205
- Yadav R, Kushari A, Eswaran V, Verma AK (2013) A numerical investigation of the Eulerian PDF transport approach for modeling of turbulent non-premixed pilot stabilized flames. *Combust Flame* 160:618–634
- Silva CV, Indrusiak MLS, Beskow AB (2010) CFD analysis of the pulverized coal combustion processes in a 160 MWe tangentially-fired-boiler of a thermal power plant. *J Braz Soc Mech Sci Eng* 32:427–436
- Krishnamoorthy G (2010) A new weighted-sum-of-gray-gases model for CO₂–H₂O gas mixtures. *Int Commun Heat Mass Transf* 37:1182–1186
- Johansson R, Leckner B, Andersson K, Johnsson F (2011) Account for variations in the H₂O to CO₂ molar ratio when modeling gaseous radiative heat transfer with the weighted-sum-of-grey-gases model. *Combust Flame* 158:893–901
- Rothman LS, Gordon IE, Barber RJ, Dothe H, Gamache RR, Goldman A, Perevalov VI, Tashkun SA, Tennyson J (2010) HITEMP, the high-temperature molecular spectroscopic database. *J Quant Spectrosc Radiat Transf* 111:2130–2150
- Kangwanpongpan T, França FHR, Silva RC, Schneider PS, Krautz HJ (2012) New correlations for the weighted-sum-of-gray-gases model in oxy-fuel conditions based on HITEMP 2010 database. *Int J Heat Mass Transf* 55:7419–7433
- Dorigon LJ, Duciak G, Brittes R, Cassol F, Galarça M, França FHR (2013) WSGG correlations based on HITEMP 2010 for computation of thermal radiation in non-isothermal, non-homogeneous H₂O/CO₂ mixtures. *Int J Heat Mass Transf* 64:863–873
- Cassol F, Brittes R, França FHR, Ezekoye OA (2014) Application of the weighted-sum-of-gray-gases model for media composed of arbitrary concentrations of H₂O, CO₂ and soot. *Int J Heat Mass Transf* 79:796–806
- Cassol F, Brittes R, Centeno FR, da Silva CV, França FHR (2015) Evaluation of the gray gas model to compute radiative transfer in non-isothermal, non-homogeneous participating medium containing CO₂, H₂O and soot. *J Braz Soc Mech Sci Eng* 37:163–172
- Snegirev AY (2004) Statistical modeling of thermal radiation transfer in buoyant turbulent diffusion flames. *Combust Flame* 136:51–71

20. Garréon D, Simonin O (1994) Final results. In: Proceedings of the 1st workshop of aerodynamics of steady state combustion chambers and furnaces 25:29–35
21. Centeno FR, Cassol F, Vielmo HA, França FHR, Silva CV (2013) Comparison of different WSGG correlations in the computation of thermal radiation in a 2D axisymmetric turbulent non-premixed methane–air flame. *J Braz Soc Mech Sci Eng* 35:419–430
22. Centeno FR, Silva CV, França FHR (2014) The influence of gas radiation on the thermal behavior of a 2D axisymmetric turbulent non-premixed methane–air flame. *Energy Convers Manag* 79:405–414
23. Silva CV, França FHR, Vielmo HA (2007) Analysis of the turbulent, non-premixed combustion of natural gas in a cylindrical chamber with and without thermal radiation. *Combust Sci Technol* 179:1605–1630
24. Magel HC, Schnell U, Hein KRG (1996) Modeling of hydrocarbon and nitrogen chemistry in turbulent combustor flows using detailed reaction mechanisms. In: Proceedings of the 3rd workshop on modeling of chemical reaction systems
25. Nieckele AO, Naccache MF, Gomes MSP, Carneiro JE, Serfaty R (2001) Models evaluations of combustion process in a cylindrical furnace. In: Proceedings of 2001 ASME IMECE
26. Patankar SV (1980) Numerical heat transfer and fluid flow. Hemisphere, Washington
27. Eaton AM, Smoot LD, Hill SC, Eatough CN (1999) Components, formulations, solutions, evaluations and applications of comprehensive combustion models. *Prog Energy Combust Sci* 25:387–436
28. Turns SR (2000) An introduction to combustion: concepts and applications. McGraw-Hill, Singapore
29. Fluent Incorporated (2009) FLUENT Theory Guide
30. Magnussen BF, Hjertager BH (1977) On mathematical models of turbulent combustion with special emphasis on soot formation and combustion. In: Proceedings of the 16th symposium (international) on combustion—The Combustion Institute, pp 719–729
31. Modest MF (1991) The weighted-sum-of-gray-gases model for arbitrary solution methods in radiative transfer. *J Heat Transf* 113:650–656
32. Bordbar MH, Wecl G, Hyppänen T (2014) A line by line based weighted sum of gray gases model for inhomogeneous CO₂–H₂O mixture in oxy-fired combustion. *Combust Flame* 161:2435–2445
33. Edge P, Gubba SR, Ma L, Porter R, Pourkashanian M, Williams A (2011) LES modelling of air and oxy-fuel pulverised coal combustion—impact on flame properties. *Proc Combust Inst* 33:2709–2716
34. Kabashnikov VP, Kmit GI (1979) Influence of turbulent fluctuations on thermal radiation. *J App Spectrosc* 31:963–967
35. Li G, Modest MF (2002) Application of composition PDF methods in the investigation of turbulence–radiation interactions. *J Quant Spectrosc Radiat Transf* 73:461–472
36. Li G, Modest MF (2002) Importance of turbulence-radiation interactions in turbulent reacting flows. In: Proceedings of 2002 ASME IMECE
37. Gupta A, Haworth DC, Modest MF (2013) Turbulence-radiation interactions in large-eddy simulations of luminous and nonluminous nonpremixed flames. *Proc Combust Inst* 34:1281–1288
38. Burns SP (1999) Turbulence radiation interaction modeling in hydrocarbon pool fire simulations. Sandia Report SAND. pp 99–3190
39. Poitou D, Amaya J, El Hafi M, Cuénot B (2012) Analysis of the interaction between turbulent combustion and thermal radiation using unsteady coupled LES/DOM simulations. *Combust Flame* 159:1605–1618
40. Centeno FR, Brittes R, França FHR, Ezekoye AO (2015) Evaluation of gas heat transfer in a 2D axisymmetric geometry using the line-by-line integration and WSGG models. *J Quant Spectrosc Radiat Transf* 156:1–11